

# DiffMI: Breaking Face Recognition Privacy via Diffusion-Driven Training-Free Model Inversion

Hanrui Wang, Shuo Wang, Chun-Shien Lu, and Isao Echizen, *Senior Member, IEEE*,

**Abstract**—Face recognition poses serious privacy risks due to its reliance on sensitive and immutable biometric data. While modern systems mitigate privacy risks by mapping facial images to embeddings (commonly regarded as privacy-preserving), model inversion attacks reveal that identity information can still be recovered, exposing critical vulnerabilities. However, existing attacks are often computationally expensive and lack generalization, especially those requiring target-specific training. Even training-free approaches suffer from limited identity controllability, hindering faithful reconstruction of nuanced or unseen identities. In this work, we propose DiffMI, the first diffusion-driven, training-free model inversion attack. DiffMI introduces a novel pipeline combining robust latent code initialization, a ranked adversarial refinement strategy, and a statistically grounded, confidence-aware optimization objective. DiffMI applies directly to unseen target identities and face recognition models, offering greater adaptability than training-dependent approaches while significantly reducing computational overhead. Our method achieves 84.42%–92.87% attack success rates against inversion-resilient systems and outperforms the best prior training-free GAN-based approach by 4.01%–9.82%. The implementation is available at <https://github.com/azrealwang/DiffMI>.

**Index Terms**—Privacy attack, model inversion, face recognition, diffusion.

## I. INTRODUCTION

Face recognition systems pose significant privacy risks due to their reliance on immutable biometric data. Large-scale leaks have occurred repeatedly, *e.g.*, U.S. CBP Cybersecurity Incident [1], U.K. Biostar 2 breach [2], Shanghai Police database leak (1B records) [3], Australia Outabox [4], and India police/military recruitment contractor leak (500GB) [5]. **As biometric data cannot be reissued like passwords, such breaches are irreversible.** To mitigate these risks, modern systems adopt system-specific feature embeddings, improving unlinkability, scalability, generalization to unseen identities, and retrieval efficiency [6]–[9]. As illustrated in Fig. 1, facial images are encoded into system-specific embeddings and compared using metrics such as cosine similarity or Euclidean distance. This approach was once considered privacy-preserving, as it obscures raw biometric information and prevents embeddings from being used across systems [10]–[13]. A widely

Hanrui Wang (corresponding author) and Isao Echizen are with Echizen Lab, National Institute of Informatics (NII), Tokyo, Japan, e-mail: {hanrui\_wang, iechizen}@nii.ac.jp. Shuo Wang is with Shanghai Jiao Tong University, Shanghai, China, e-mail: wangshuo@sjtu.edu.cn. Chun-Shien Lu is with Institute of Information Science, Academia Sinica, Taipei, Taiwan. e-mail: lcs@iis.sinica.edu.tw.

This work was partially supported by JSPS KAKENHI Grants JP21H04907 and JP24H00732, by JST CREST Grant JPMJCR20D3 and JPMJCR2562 including AIP challenge program, by JST AIP Acceleration Grant JP-MJCR24U3, and by JST K Program Grant JPMJKP24C2 Japan.

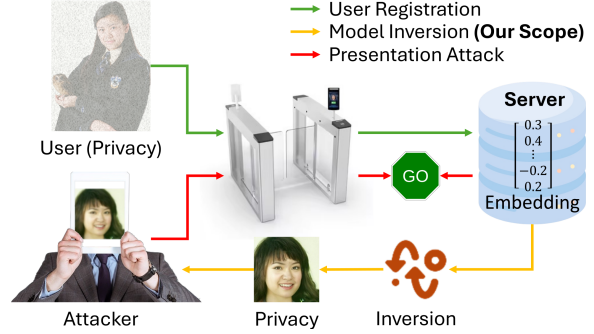


Fig. 1: The threat of model inversion against embedding-based face recognition systems. Although such systems store embeddings instead of raw images for privacy protection, model inversion attacks can reconstruct facial images directly from embeddings, enabling downstream threats such as presentation attacks that can bypass authentication.

adopted evaluation protocol for privacy risk measures whether leaked info reveals transferable identity information, which would constitute a privacy breach [14]–[18].

However, recent model inversion attacks show that facial images can be reconstructed from embeddings alone, enabling threats such as identity spoofing in biometric authentication (*e.g.*, unlocking smartphones or accessing secure facilities), surveillance and re-identification in public datasets, and long-term identity theft. As illustrated in Fig. 1, even without raw photos, recovering a face from an embedding may allow attackers to forge IDs, impersonate users in video calls, or bypass bans on reusing facial data [33], [34]. Understanding these inversion risks is thus critical for assessing the real-world security of embedding-based systems [14].

While attacks have demonstrated the feasibility, they continue to face several **key challenges**.

(i) *Training-Dependent*: Most prior attacks are training-dependent, as listed in Tab. I, requiring the training or fine-tuning of a target-specific generator. Such strategy incurs substantial computational overhead while offering limited generalizability [15]–[17], [19]–[29]. Note that inversion attacks require a generative model; we therefore distinguish a *training-free* setting, where a single fixed generator is reused across all targets, from a *training-dependent* setting, where a separate generator is trained or fine-tuned for each target.

Moreover, many training-dependent attacks target closed-set identity classification, where adding or removing identities requires retraining the recognition model. These attacks rely on task-specific training over a fixed set of identities (*i.e.*, seen

TABLE I: Representative model inversion attacks, highlighting both influential early methods and recent advances.

Method	Generator	Attack Cost	Reference <sup>1</sup>	Threat Model <sup>2</sup>	Task	Visual Fidelity		Code
		Training-Free			Open-Set	Image Size <sup>3</sup>	Selfies	
MIA [19] [2015]	None	✗	Ⓐ	□ & ⚡	✗	■	✗	✓
NbNet [20] [2018]	DeconvNet	✗	Ⓑ	■	✓	■ 160	✗	✓
Amplified-MIA [21] [2023]	DeconvNet	✗	Ⓐ	■	✗	■ 64	✗	✓
DSCasConv [15] [2024]*	DeconvNet	✗	Ⓑ	□	✓	■ 112	✗	✓
DiBiGAN [22] [2020]	C-GAN	✗	Ⓑ	□ & ⚡	✓	■ 64	✗	✗
GMI [23] [2020]	C-GAN	✗	Ⓐ	□	✗	■ 64	✗	✓
$\alpha$ -GAN [24] [2022]	C-GAN	✗	Ⓐ	□	✗	■	✗	✗
PLG-MI [25] [2023]	C-GAN	✗	Ⓐ	□	✗	■ 64	✗	✓
LOKT [26] [2023]	C-GAN	✗	Ⓐ	■	✗	■ 128	✗	✓
ABE-MI [27] [2025]	C-GAN	✗	Ⓐ	■	✗	■ 128	✗	✗
ID3PM [28] [2023]	C-Diffusion	✗	Ⓑ	■	✓	■ 64	✓	✗
CDM [29] [2024]	C-Diffusion	✗	Ⓐ	■	✗	■ 64	✗	✗
Shahreza <i>et al.</i> [16] [2023]	StyleGAN	✗	Ⓑ	□ & ⚡	✓	■ 1024	✓	✓
Shahreza <i>et al.</i> [17] [2024]*	StyleGAN	✗	Ⓑ	□ & ⚡	✓	■ 1024	✓	✓
PPA [30] [2022]	StyleGAN	✓	Ⓐ	□	✗	■ 1024	✓	✓
IF-GMI [31] [2024]	StyleGAN	✓	Ⓐ	□	✗	■ 224	✗	✓
Dong <i>et al.</i> [18] [2023]	StyleGAN	✓	Ⓑ	■	✓	■ 1024	✓	✗
MAP <sup>2</sup> V [14] [2024]*	StyleGAN	✓	Ⓑ	□ & ⚡	✓	■ 192	✗	✓
PriDM [32] [2025]	DDPM	✓	■	■	✗	■ 256	✓	✗
<b>DiffMI (Ours)</b>	DDPM	✓	Ⓑ	□ & ⚡	✓	■ 256	✓	✓

<sup>1</sup> Ⓐ Label Ⓑ Embedding Ⓒ Partial raw facial image <sup>2</sup> □ White-Box ■ Black-Box □ & ■ Both <sup>3</sup> ■ Grayscale ■ RGB

\* Indicates benchmark methods used for empirical comparison, selected as representative exemplars of each strategy. We exclude attack approaches targeting closed-set identity classification models, as well as PriDM [32], which requires partial target images and therefore demands significantly more information than is permitted under our threat model.

models and seen identities) [19], [21], [23]–[27], [29]–[31]. In contrast, modern face recognition systems are embedding-based and open-set by design, supporting generalization to unseen identities and dynamic user enrollment without retraining. As a result, closed-set attacks are poorly aligned with real-world deployment scenarios.

Additionally, high-fidelity reconstruction remains challenging for training-dependent methods due to their substantial training overhead [15], [19]–[29]. Effective identity recovery requires visually rich, high-resolution outputs (ideally with larger image size and full headshot-style, *a.k.a.* selfie, reconstructions) [16]–[18], [30]. As shown in Tab. I, training-free methods more easily achieve this, while training-dependent ones often produce only low-resolution (*e.g.*, 64×64) or grayscale facial crops, insufficient for reliable recognition.

(ii) *Limited Identity Controllability*: Even training-free, GAN-based attacks suffer from limited identity controllability [14], [18], [30], [31]. Despite the prevalence of diffusion models in modern generative systems [35], training-free inversion attacks still largely rely on GANs [36], which are typically constrained by a truncation radius to suppress artifacts, limiting fine-grained identity control.

(iii) *Adversarial Overfitting*: Naively adapting GAN-style inversion to diffusion causes severe artifacts and overfitting. A simple training-free approach applies adversarial attacks directly in the diffusion latent space, but such updates often push latents off the Gaussian prior, causing the reverse denoising process to amplify off-manifold signals into halos, patchy textures, and model-specific overfitting. These artifacts may even mislead the target model into falsely confirming

reconstruction success. Consequently, prior diffusion-based attacks rely on *conditional* generation, which requires target-specific training, days of computation, and yields only low-resolution results [28], [29].

**Contributions:** Addressing these limitations requires a training-free approach that can guide unconditional diffusion models toward identity-consistent reconstructions while suppressing overfitting-induced artifacts. Our contributions are summarized as follows:

- **The first diffusion-driven, training-free model inversion.** We introduce DiffMI, the first diffusion-driven, training-free inversion attack on embedding-based face recognition. It uses a fixed, pretrained diffusion model to generate full headshot-style images directly from embeddings, without target-specific generator training.
- **A novel pipeline.** We identify three key factors for success: robust latent initialization, fine-grained adversarial manipulation, and artifact suppression. Our pipeline integrates automated robust latent code selection, a ranked adversarial refinement strategy, and a statistically grounded confidence-aware objective. These components enable precise latent-space updates with principled stopping to avoid overfitting, supporting attacks on unseen identities and models.
- **State-of-the-art performance.** On two datasets [38], [39] and four recognition models [10]–[13], DiffMI exceeds the best prior training-free baseline [14] by +8.97% in identity match accuracy. It also compromises inversion-resilient systems [12], [13], achieving 84.42%–92.87% success rates, revealing critical vulnerabilities in current

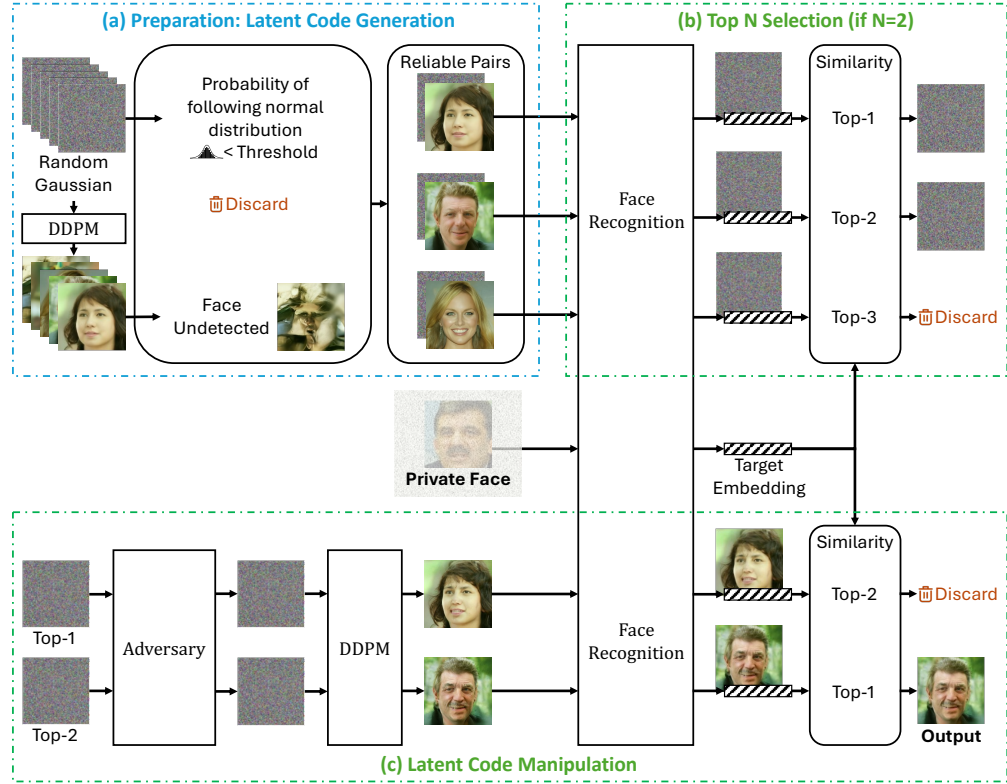


Fig. 2: Framework of DiffMI, which reconstructs a facial image sharing the same identity as a private face solely from its embedding. The generator, a denoising diffusion model (DDPM) [37], is pretrained independently, without prior knowledge of the private face or the target model. In Step (a), a set of highly robust latent codes is generated once and reused for any target. In Step (b),  $N$  codes whose reconstructions have the highest similarity to the target embedding are selected as initialization for Step (c). In Step (c), these codes undergo adversarial refinement to progressively align the reconstructions with the target embedding. Notably, a higher initial rank does not guarantee superior final reconstruction after refinement.

privacy defenses. We further conduct *user studies* in which participants assess whether reconstructions match target identities.

## II. DIFFUSION-DRIVEN MODEL INVERSION (DIFFMI)

This section introduces DiffMI. Sec. II-B outlines the objectives and overall framework (Fig. 2). Sec. II-C formalizes the problem and defines the objective function. The three core algorithmic components, latent code initialization, selection, and manipulation, are detailed in Secs. II-D to II-F. Notations are summarized in the supplementary materials.

### A. Threat Model

DiffMI functions as an attacker that assesses the privacy vulnerabilities of a face recognition model. Specifically, it examines whether a facial image reconstructed solely from a feature embedding can visually resemble the identity represented by that embedding.

*a) Attack Knowledge:* The attacker's level of access determines the threat model:

- *White-box:* Access to both the target embedding and model gradients.
- *Black-box:* Access to the target embedding and model outputs via queries.

In embedding-based recognition, the attacker has no access to identity labels, raw images, or original latent features, only the embedding.

*b) Attack Objective:* We aim to reconstruct a face that enables recognition of the target identity, assessed via two criteria:

- The reconstruction is visually perceived as depicting the same person as the target.
- The reconstruction enables identification of the target among a set of identities.

While visual similarity is inherently subjective and best assessed via user studies, we complement human evaluation with automated metrics using face recognition. Because adversarial optimization may introduce artifacts exploiting model-specific weaknesses, we assess DiffMI's effectiveness through *cross-model robustness*, a widely adopted privacy risk metric measuring whether reconstructed faces achieve transferable identity alignment across *non-target models* [14]–[18]. Formally, the attack is defined by two objectives:

- *During optimization:* Maximize the embedding similarity between the reconstruction and the target until a predefined confidence threshold is reached.
- *During evaluation:* Ensure the output is recognized as the target identity by non-target models, including when

compared to non-target images of the target identity.

### B. Overview

DiffMI is a training-free framework for assessing the privacy risks of embedding-based face recognition models. A model is deemed vulnerable if DiffMI can reconstruct a facial image resembling the target identity from its feature embedding alone. The goal is to recover the identity associated with the embedding, not the original input image. Built on DDPM [37], a pretrained unconditional face generator, DiffMI generalizes to unseen target models and identities.

The key challenge is guiding unconditional diffusion toward identity-consistent outputs while suppressing adversarial artifacts. We address this with a **confidence-aware objective** that enables early stopping to prevent overfitting, coupled with the following three-step procedure (Fig. 2):

a) *Step (a) – Robust Latent Code Initialization (Independent Preparation)*: A pool of robust latent codes is prepared for reuse in subsequent attacks. Robustness is enforced via a dual-selection strategy: D’Agostino’s  $K^2$  test [40]–[42] ensures Gaussian normality of the latent distribution, and MTCNN [43] verifies the presence of facial features in the initial generations. These filters improve initialization quality and resistance to optimization-induced distortion.

b) *Step (b) – Top N Latent Code Selection*: From the filtered pool, the top  $N$  codes are selected by embedding similarity between their generated images and the target. This provides stronger identity alignment before manipulation, even if the images are not yet close matches.

c) *Step (c) – Ranked, Fine-Grained Latent Code Manipulation*: The selected codes undergo fine-grained adversarial optimization to maximize confidence-aware embedding similarity with the target. A confidence threshold enables early stopping once the similarity score on the target model reaches a statistically grounded level, indicating sufficient refinement for cross-model robustness. A ranked adversary strategy, guided by similarity priorities and the confidence-aware objective, improves computational efficiency and mitigates overfitting-induced artifacts.

### C. Problem Definition and Objective Function

Embedding-based face recognition models map input images  $x$  to  $d$ -dimensional embeddings  $z = F(x) \in \mathbb{R}^d$ , where  $F(\cdot)$  denotes the embedding function representing the face recognition model. Two images are classified as the same identity if the cosine similarity of their embeddings satisfies:  $S(z_1, z_2) = \frac{z_1 \cdot z_2}{\|z_1\| \|z_2\|} \geq \tau_F$ , where  $\tau_F$  is the decision threshold optimized for the minimum equal error rate (EER).

Given a target face  $x^{\text{tgt}}$  and target model  $F(\cdot)$ , DiffMI seeks to reconstruct an image  $\hat{x}$  sharing the identity of  $x^{\text{tgt}}$ , using only its embedding  $z^{\text{tgt}} = F(x^{\text{tgt}})$ . The objective is identity preservation rather than pixel-level fidelity:

$$S(F(\hat{x}), F(x^{\text{tgt}})) \geq \tau_F. \quad (1)$$

The reconstruction  $\hat{x}$  is produced by a pretrained DDPM [37], modeled as a generative function  $G(\cdot)$  applied to a latent code  $x_G$  drawn from a standard Gaussian distribution:

$$\hat{x} = G(x_G), \quad x_G \sim \mathcal{N}(0, I). \quad (2)$$

Substituting into Eq. (1) gives:

$$S(F(G(x_G)), F(x^{\text{tgt}})) \geq \tau_F. \quad (3)$$

Since a randomly sampled  $x_G$  rarely satisfies Eq. (3), we introduce an adversarial perturbation  $\delta$ , constrained by an  $L_p$ -norm bound  $\epsilon$ , to optimize  $x_G$ :

$$x'_G = x_G + \delta, \quad \text{s.t. } \|\delta\|_p \leq \epsilon, \quad (4)$$

yielding the refined objective:

$$S(F(G(x_G + \delta)), F(x^{\text{tgt}})) \geq \tau_F. \quad (5)$$

Therefore, the objective function  $\mathcal{L}$  is defined via Eq. (5):

$$\mathcal{L} = S(F(G(x_G + \delta)), F(x^{\text{tgt}})). \quad (6)$$

The goal is to iteratively update  $\delta$  to maximize  $\mathcal{L}$ :

$$\delta = \arg \max_{\|\delta\|_p \leq \epsilon} \mathcal{L}. \quad (7)$$

**Confidence-Aware Objective** As shown in Fig. 3, stable cross-model robustness requires the similarity score  $\mathcal{L}$  to substantially exceed the target model’s decision threshold  $\tau_F$ . Although the objective in Eq. (7) steadily increases  $\mathcal{L}$  on the target model, further updates beyond a certain point (e.g.,  $\mathcal{L} > 0.98$ ) offer negligible gains while degrading generalization. This indicates that blindly maximizing  $\mathcal{L}$  adds unnecessary computation and risks overfitting to the target model.

To address this, we propose a *confidence-aware objective* with an early stopping criterion. A confidence threshold  $\tau_C$  is set, and optimization terminates once  $\mathcal{L} \geq \tau_C$ . This threshold is a statistically grounded upper bound on the maximum similarity observed between real images of the same identity under the target model:

$$\tau_C = \max S(F(x^i), F(x^{j \neq i})), \quad x^i, x^j \in \mathcal{X}_{\text{real}}. \quad (8)$$

Fig. 3 demonstrates that stopping the optimization at approximately  $\tau_C = 0.98$  reduces unnecessary computation while retaining optimal cross-model robustness.

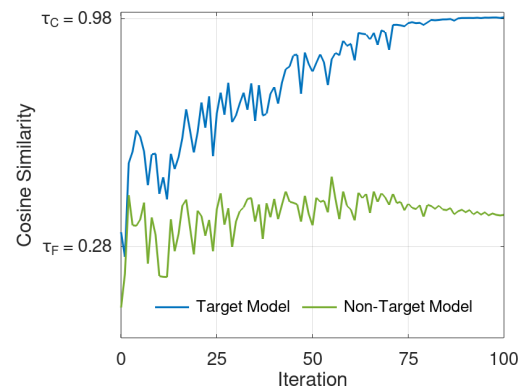


Fig. 3: Optimization convergence on the target model and cross-model robustness on the non-target model. To achieve stable cross-model robustness, the optimization must push  $\mathcal{L}$  well beyond the target model’s decision threshold  $\tau_F$ . However, once  $\mathcal{L} > \tau_C$ , further updates yield diminishing improvements in similarity while degrading cross-model robustness.

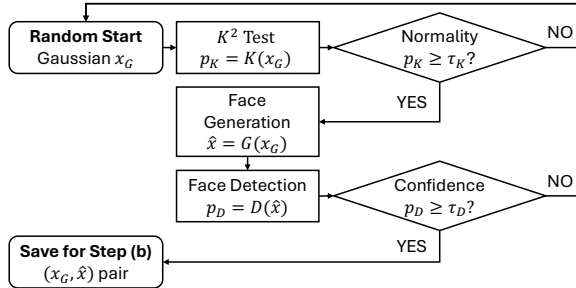


Fig. 4: Two-stage latent code generation. First,  $K^2$  test  $K(\cdot)$  [40]–[42] filters each sampled latent code  $x_G$  based on Gaussian normality, retaining those with  $p_K \geq \tau_K$ . Then, MTCNN  $D(\cdot)$  [43] verifies whether the corresponding image  $\hat{x} = G(x_G)$  contains a detectable face, accepting codes with detection confidence  $p_D \geq \tau_D$ .

#### D. Step (a) – Latent Code Initialization

We adopt a two-stage strategy to generate robust latent codes for initialization (Fig. 4), ensuring both statistical validity and visual plausibility. This involves filtering with D’Agostino’s  $K^2$  test [40]–[42] for Gaussianity and verifying facial presence via MTCNN [43]. Step (a) is performed once to build a reusable pool of high-quality latent codes applicable across different targets. Enforcing both statistical and perceptual constraints ensures robust initialization, reducing susceptibility to distortion during later adversarial optimization.

The process proceeds sequentially: sampled latent codes are first screened via the  $K^2$  test, a lightweight check discarding those deviating from the Gaussian prior. Remaining codes are then denoised into images  $\hat{x} = G(x_G)$  and passed through MTCNN for face detection, a more computationally expensive step. This ordering improves efficiency, as statistically valid codes are likelier to yield recognizable faces.

1) *Normality Test via D’Agostino’s K-Square Statistic:* Reconstructing facial images with DDPM requires latent codes of size  $3 \times 256 \times 256$  to follow a normal distribution (*i.e.*, Gaussian normality) [37]. The normality of randomly sampled codes varies and generally correlates with reconstruction quality. However, even highly normal codes will be pushed off this manifold by adversarial manipulation, with deviations amplified during denoising and leading to visual artifacts. Evidence of normality variance and its deterioration after manipulation is shown in Figs. 11 and 12 in ablation.

To alleviate this, we apply D’Agostino’s  $K^2$  test [40]–[42] to select codes with strong initial normality, thereby enhancing baseline image quality and preserving fidelity during optimization. Given a latent code  $x_G$ , the  $K^2$  test function  $K(\cdot)$  computes a  $p$ -value based on skewness and kurtosis:

$$p_K = K(x_G). \quad (9)$$

We retain codes satisfying the normality threshold  $\tau_K$ :

$$x_G \text{ is selected if } p_K \geq \tau_K. \quad (10)$$

Since latent sampling is inexpensive, a strict threshold can be enforced without limiting code availability. This filtering step

ensures selected codes adhere closely to Gaussian properties, improving robustness to subsequent adversarial perturbations.

2) *Face Detection via MTCNN:* Latent codes satisfying Gaussian normality may still fail to produce recognizable faces (see examples in Fig. 13 in ablation). We use MTCNN [43], a deep learning-based face detector, to ensure the presence of facial features.

Given a latent code  $x_G$ , the DDPM generator  $G(\cdot)$  produces the corresponding image:

$$\hat{x} = G(x_G). \quad (11)$$

We then apply the face detector  $D(\cdot)$ , which returns a confidence score  $p_D$  indicating the likelihood of a detected face:

$$p_D = D(\hat{x}). \quad (12)$$

Latent codes are accepted if their detection confidence exceeds a predefined threshold  $\tau_D$ :

$$(x_G, \hat{x}) \text{ is selected if } p_D \geq \tau_D. \quad (13)$$

Since most latent codes passing  $K^2$  test already yield plausible facial structures, a relatively high  $\tau_D$  can be used without significantly reducing the acceptance rate. To support later stages, both  $x_G$  and  $\hat{x}$  are cached for efficient reuse.

#### E. Step (b) – Latent Code Selection

Step (a) yields  $V$  robust latent codes and their reconstructions,  $\{(x_{G_v}, \hat{x}_v)\}_{v=1}^V$ . Selecting the single code with the highest initial similarity to the target embedding minimizes computation but may underperform after adversarial optimization (see examples in Fig. 14 in ablation). To address this, DiffMI selects the top  $N$  candidates ( $N \leq V$ ) ranked by identity similarity (Fig. 5). Larger  $N$  generally improves inversion success at the cost of higher computation.

Specifically, each reconstruction  $\hat{x}_v = G(x_{G_v})$ , precomputed in Step (a), is passed through the target model  $F(\cdot)$  to obtain an embedding. Cosine similarity (Eq. (6)) is then computed between this embedding and the target embedding  $z^{tgt}$ . The top  $N$  latent codes with the highest similarity scores are retained as initialization points for Step (c).

In the black-box setting (Sec. II-A), Step (b) requires  $V$  model queries, one per candidate:

$$Q_{TopN} = V, \quad (14)$$

where  $V$  is the number of latent code candidates. Notably, the cost in Step (b) is  $V$  rather than  $N$ , as it requires computing similarity scores between all  $V$  latent codes and the target embedding in order to select the top  $N$  candidates.

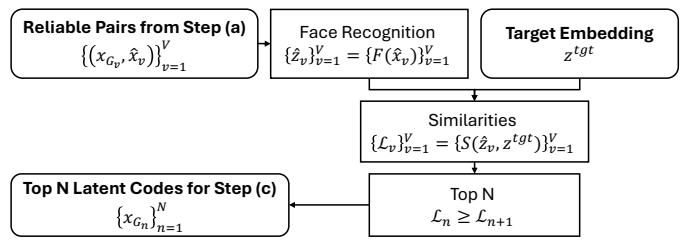


Fig. 5: Selection of the top  $N$  latent codes based on embedding similarity to the target identity.

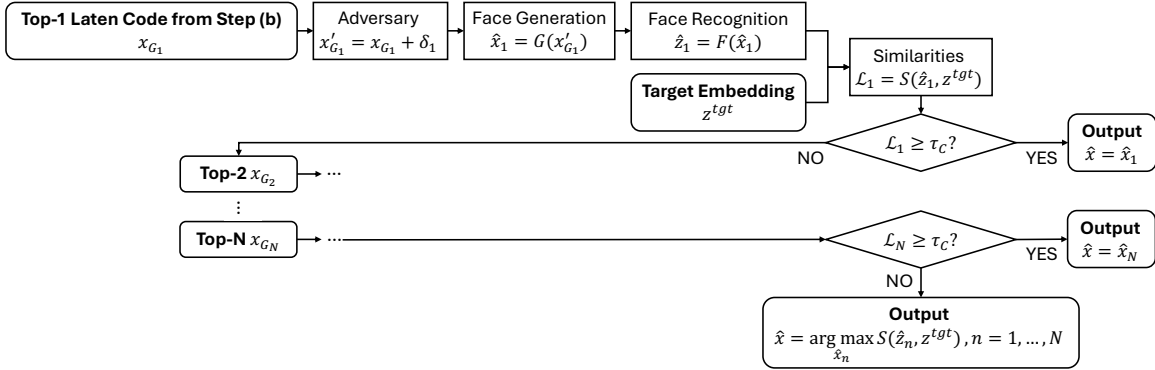


Fig. 6: Ranked Adversary algorithm for latent code manipulation. The top  $N$  latent codes, ranked in Step (b), are sequentially optimized via adversarial manipulation to maximize the objective in Eq. (6). The process terminates early if any code satisfies  $\mathcal{L}_n \geq \tau_C$  for  $n = 1, \dots, N$ . If none meet the confidence threshold  $\tau_C$ , the code  $x'_G$  with the highest  $\mathcal{L}_n$  is selected, and its reconstruction is returned as the final facial image.

#### F. Step (c) – Latent Code Manipulation

Randomly sampled latent codes, even those close to the target embedding, typically require refinement to satisfy the identity-matching objective. Prior methods either refine only the top-1 code or fuse the top  $N$  candidates [14], but fusion often reduces identity similarity and shares the same failure modes as single-code strategies, where the best initial match does not guarantee the best final result.

To address these limitations, we propose the *Ranked Adversary* strategy: a ranking-based refinement approach that sequentially optimizes the top  $N$  latent codes, prioritizing those with higher initial similarity. This avoids fusion, preserves candidate diversity, and enables early stopping via the confidence-aware objective.

1) *Ranked Adversary*: The Ranked Adversary algorithm (Fig. 6) sequentially refines the top  $N$  latent codes obtained from Step (b), starting with the highest-ranked code  $x_G$ . Each code is updated adversarially to maximize identity similarity, as defined in Eq. (6).

The process stops early if any refined code satisfies the confidence threshold, *i.e.*,  $\mathcal{L}_n \geq \tau_C$  for some  $n \in \{1, \dots, N\}$ , returning  $\hat{x}_n = G(x_G + \delta_n)$  as the final reconstruction. If no code reaches the threshold within the maximum number of iterations  $t_{\max}$ , the code with the highest final similarity is selected, and its reconstruction is returned as the output.

2) *Fine-Grained Adversarial Learning*: Effective manipulation of unconditional diffusion generation does not require novel adversarial architectures, but rather a fine-grained optimization strategy. As defined by Wang *et al.* [44], fine-grained adversarial attacks operate at a localized, precision-controlled level, enabling gradual refinement in high-dimensional latent spaces. In our framework, the Ranked Adversary employs APGD [45] for white-box and GreedyPixel [44] for black-box settings.

While alternative coarse-grained methods can be integrated into our manipulation pipeline, empirical results (Fig. 10) show that only fine-grained techniques consistently produce high-quality reconstructions without significant visual artifacts. This behavior stems from the sensitivity of the diffusion model's latent space: even small off-manifold perturbations

can propagate through the denoising process and amplify into perceptible degradation. Unlike classifier-based models, where local smoothness may tolerate coarse updates, the iterative nature of diffusion models compounds small inconsistencies, making precision essential.

3) *Query Efficiency in the Black-Box Setting*: In the black-box setting, query cost arises from evaluating the objective function in Eq. (6), which requires querying the target model to obtain embeddings of reconstructed images. Consequently, the total query cost is proportional to the number of adversarial iterations.

For a single latent code, the query cost is:

$$Q_{\text{Adv}} \leq t_{\max}, \quad (15)$$

where  $t_{\max}$  is the maximum number of adversarial iterations. Since the Ranked Adversary may process up to  $N$  latent codes, the total query cost for the manipulation phase is bounded by:

$$Q_{\text{Adv}} \leq N \times t_{\max}. \quad (16)$$

Including the  $V$  queries for top- $N$  latent code selection in Step (b) (Eq. (14)), the total query complexity of DiffMI is:

$$Q = Q_{\text{Top}N} + Q_{\text{Adv}}. \quad (17)$$

In practice, black-box attacks are constrained by a strict query budget  $Q_{\max}$ . To satisfy this constraint, the number of iterations per latent code must be bounded by:

$$t_{\max} = \left\lfloor \frac{Q_{\max} - V}{N} \right\rfloor, \quad (18)$$

where  $\lfloor \cdot \rfloor$  denotes the floor function, and  $V$  is the number of latent codes evaluated in Step (b). This formulation enables precise control over query consumption while maintaining optimal attack effectiveness within the given budget.

### III. EXPERIMENTAL SETTINGS

Model architectures and datasets are summarized in Tab. II. White-box configurations are summarized in Tab. III, and black-box settings are illustrated in Fig. 10. All experiments are conducted on an NVIDIA A100 GPU.

TABLE II: Diversity of Model Architectures and Datasets.

Model	Architecture	Training Dataset	Attack Dataset	Comment
FaceNet [10]	InceptionResNetV1	VGGFace2 [46]	LFW [39] ( <b>Major</b> ) CelebA-HQ [38]	One target model; three for cross-model evaluation
ArcFace [11]	IResNet100	MS1MV2 [47]		
DCTDP [12]	ResNet50	VGGFace2 [46]		
PartialFace [13]	IResNet50	MS1MV2 [47]		
DSCasConv [15]	DeconvNet	FFHQ [48]		Training-dependent generator
StyleGAN [36]	StyleGAN	FFHQ [48]		Training-free generator
DDPM [37]	UNet	CelebA-HQ [38]		Training-free generator ( <b>Ours</b> )

TABLE III: Configurations of target models and DiffMI.

Face Recognition	$\tau_F$	Latent Code Generation	$\tau_K$	$\tau_D$	Latent Code Manipulation	$\tau_C$	Norm	$\epsilon$
FaceNet [10]	0.40				0.99			25
ArcFace [11]	0.23				0.99			35
DCTDP [12]	0.26	1,000	0.999	0.999	3	100	0.98	35
PartialFace [13]	0.28						0.98	35

$\tau_F$ : Identity similarity threshold, set to minimize EER;  $\tau_K$ : Gaussian normality threshold;  $\tau_D$ : Detection confidence threshold;  $\tau_C$ : Optimization confidence threshold, computed in Eq. (8).

### A. Face Recognition Models

We evaluate inversion attacks on two widely used face recognition models: FaceNet [10] and ArcFace [11]; as well as two inversion-resilient models: DCTDP [12] and PartialFace [13], both designed to mitigate inversion. Decision thresholds are set at the minimum EER for each model, as detailed in Tab. III.

### B. Datasets

We conduct evaluations on the LFW [39] and CelebA-HQ [38] datasets. Each dataset is subsampled to 1,000 images (10 images from 100 identities). Since DiffMI is training-free, evaluation result variance is largely independent of dataset size; thus, 1,000-image subsets suffice for fair comparison, provided the evaluation sets are disjoint from both generator and target model training data. Datasets lacking identity labels, such as FFHQ [48], are excluded.

### C. Baselines

We compare DiffMI with three representative model inversion attacks spanning key design paradigms: a training-free GAN-based method (MAP<sup>2</sup>V) [14], a training-dependent DeconvNet-based method [17], and a training-dependent GAN-based method [15]. These baselines capture the diversity of prior approaches across training-free and training-dependent settings. Closed-set attacks requiring target-specific training on a limited set of predefined identities are excluded.

### D. User Study

Following the objectives in Sec. II-A, we conducted a user study with ten participants<sup>1</sup> tasked to: (i) judge whether

<sup>1</sup>*Ethical Statement:* No personal data was collected. All identities and images were sourced from public datasets (LFW and CelebA) or generated by our method, ensuring no privacy concerns.



Fig. 7: Example of difficult identity selection in the user study. Each candidate is represented by two photos; three identities are shown in randomized order. Several participants noted that the first two male candidates appeared too similar, complicating the task.

a reconstructed image depicts the same individual as the target (a straightforward matching task relevant to identity authentication); and (ii) identify the target individual from a candidate pool based on the reconstruction (mimicking witness identification in forensic scenarios). Each session comprised 60 images/identities from LFW and CelebA-HQ (MAP<sup>2</sup>V evaluated with only 30). To increase difficulty, distractors were chosen with embedding similarity  $\approx 80\% \times \tau_F$  (see Fig. 7), making them visually ambiguous.

### E. Evaluation Metrics

We evaluate privacy leakage using Type I and Type II accuracies [20], with Type II accuracy serving as the primary metric due to its stricter exclusion of the target image used during attack optimization. Higher values in both metrics indicate stronger identity recovery and greater privacy compromise.

**Type I accuracy** measures how often a reconstructed image  $\hat{x}$  matches the exact target image  $x_i^{\text{tgt}}$  in the embedding space of a face recognition model  $F(\cdot)$ :

$$\text{Type I} = \frac{1}{I} \sum_{i=1}^I \mathbb{I}(S(F(\hat{x}_i), F(x_i^{\text{tgt}})) \geq \tau_F), \quad (19)$$

where  $S(\cdot, \cdot)$  denotes cosine similarity,  $\tau_F$  is the identity matching threshold, and  $\mathbb{I}(\cdot)$  is the indicator function.

**Type II accuracy** evaluates whether  $\hat{x}$  matches other images of the same identity, excluding  $x_i^{\text{tgt}}$ . This reduces overfitting and simulates real-world scenarios where an attacker leverages biometric leakage to compromise unrelated systems:

$$\text{Type II} = \frac{1}{I \times J} \sum_{i=1}^I \sum_{j=1}^J \mathbb{I}(S(F(\hat{x}_i), F(x_i^{j \neq \text{tgt}})) \geq \tau_F), \quad (20)$$

where  $J$  is the number of alternative images per identity.

TABLE IV: Privacy vulnerabilities of face recognition models evaluated under DiffMI.

Dataset	Target Model	Evaluation									
		FaceNet		ArcFace		DCTDP		PartialFace		Average	
		Type I	Type II	Type I	Type II	Type I	Type II	Type I	Type II	Type I	Type II
CelebA	FaceNet	100.00	96.93	96.70	80.12	97.90	84.19	94.90	77.67	97.38	84.73
	ArcFace	99.90	92.76	100.00	99.06	100.00	94.23	99.90	92.84	99.95	94.72
	DCTDP	99.30	87.43	99.50	89.62	100.00	96.52	99.90	86.61	99.68	90.05
	PartialFace	97.70	80.06	99.20	87.29	99.60	85.82	100.00	96.14	99.13	87.33
LFW	FaceNet	100.00	98.56	87.00	66.23	93.40	73.31	80.80	59.92	90.30	74.51
	ArcFace	96.00	91.03	100.00	99.64	99.60	95.88	98.60	92.33	98.55	94.72
	DCTDP	96.70	90.34	99.70	95.37	100.00	99.44	97.80	86.31	98.55	92.87
	PartialFace	90.90	75.39	98.70	85.44	96.20	77.99	100.00	98.84	96.45	84.42

Gray cells indicate evaluation on target models. Green and red highlight the most and least secure models, with the lowest and highest accuracies, respectively.

**Takeaway:** FaceNet [10] exhibits the strongest privacy protection, outperforming even inversion-resilient models such as PartialFace [13] and DCTDP [12], while ArcFace [11] shows the weakest resistance to inversion attacks.

#### F. Evaluation Protocol

Since model inversion attacks optimize directly against a specific recognition model, outputs may overfit, appearing successful due to adversarial artifacts. We treat such overfitting as failure. To robustly assess privacy risk and reduce model-specific bias, we report *average cross-model accuracy over both target and non-target models*.

As described earlier, we evaluate four face recognition models. In each attack instance, one model serves as the *target* (*i.e.*, used for optimization), while the remaining three act as *non-target* models to test generalization. This setup assesses whether identity leakage transfers across architectures.

To ensure consistency and avoid bias from model-specific variability (*e.g.*, comparing the average of Models A+B+C with target D vs. B+C+D with target A), we report results *averaged over all four models* (*i.e.*, always the average of Models A+B+C+D), regardless of which model is targeted. This provides a more reliable measure of each model’s vulnerability, treating the target model as a biometric system that can also be compromised, rather than excluding it, thereby better reflecting the attack’s generalizability.

## IV. EVALUATION

### A. White-Box Model Inversion

#### 1) Privacy Vulnerabilities of Face Recognition Models:

We begin by evaluating the privacy vulnerabilities of face recognition models under the proposed DiffMI attack in the white-box setting (setup refers to Tab. III). As shown in Tab. IV, DiffMI successfully compromises all four models, including inversion-resilient variants, with Type I accuracies ranging from 90.30% to 99.95% and Type II accuracies from 74.51% to 94.72% across two datasets.

Interestingly, models explicitly designed for inversion resistance (PartialFace and DCTDP) do not demonstrate superior robustness. In contrast, FaceNet, the oldest and standard model, exhibits the strongest resistance, challenging the effectiveness of current inversion-resilient defenses.

**User Study** To validate that our high quantitative results are not solely due to adversarial overfitting, we conducted a

TABLE V: User study results with PartialFace [13] as the target (inversion-resilient) model.

Question	Dataset	Accuracy (%) ↑
Same person?	LFW	71.5 (14.3 / 20.0)
Which one matches?	LFW	80.5 (16.1 / 20.0)
Which one matches?	CelebA	81.0 (16.3 / 20.0)

user study to assess whether human perceptual judgments align with the reported Type II accuracies. Participants were asked two questions: (*i*) “Do you think the reconstruction and target depict the same person?”; and (*ii*) “Given three candidates (each with two reference photos), which one matches the reconstruction?”

Results in Tab. V confirm the attack’s practical effectiveness: over 71.5% of reconstructions were correctly matched to their identities by human participants, further supporting the real-world privacy threat posed by DiffMI.

**2) Comparison with Training-Free Baseline:** As summarized in Tab. I, existing training-free model inversion methods are all GAN-based. DiffMI represents the first diffusion-driven, training-free approach. We compare DiffMI against the strongest prior method, MAP<sup>2</sup>V [14].

As shown in Tab. VI, DiffMI consistently surpasses MAP<sup>2</sup>V in both Type I and Type II accuracies and attains higher similarity convergence. This demonstrates that diffusion-based generation enables more accurate identity reconstruction than GANs, despite both being training-free.

Moreover, the similarity scores of DiffMI approach the confidence threshold  $\tau_C$ , a statistically grounded upper bound reflecting the performance of real facial images. This convergence underscores the superior identity fidelity of diffusion models.

We also compare qualitative results in Fig. 8. Visually, DiffMI achieves higher identity resemblance and generates full headshot-style reconstructions, offering finer granularity for identity recovery than MAP<sup>2</sup>V.

**3) Comparison with Training-Dependent Baselines:** Although our proposed DiffMI is training-free, making it signif-

TABLE VI: Performance comparison between DiffMI and the training-free baseline MAP<sup>2</sup>V [14] on four face recognition models.

Dataset	Attack	FaceNet			ArcFace			DCTDP			PartialFace		
		Type I	Type II	Similarity <sup>3</sup>	Type I	Type II	Similarity <sup>3</sup>	Type I	Type II	Similarity <sup>3</sup>	Type I	Type II	Similarity <sup>3</sup>
CelebA	Original <sup>1</sup>	100.00	97.00	$\tau_C = 0.99$	100.00	99.09	$\tau_C = 0.99$	100.00	96.62	$\tau_C = 0.98$	100.00	95.65	$\tau_C = 0.98$
	Random <sup>2</sup>	4.40	4.50	0.0822	1.30	1.73	0.0304	4.20	4.74	0.0771	10.10	9.72	0.1404
	MAP <sup>2</sup> V	89.75	69.19	0.9248	95.03	84.61	0.8175	96.75	81.12	0.8135	97.98	80.84	0.7758
LFW	Ours	<b>97.38</b>	<b>84.73</b>	<b>0.9920</b>	<b>99.95</b>	<b>94.72</b>	<b>0.9898</b>	<b>99.68</b>	<b>90.05</b>	<b>0.9818</b>	<b>99.13</b>	<b>87.33</b>	<b>0.9818</b>
	Original <sup>1</sup>	100.00	98.60	$\tau_C = 0.99$	100.00	99.62	$\tau_C = 0.99$	100.00	99.47	$\tau_C = 0.98$	100.00	98.89	$\tau_C = 0.98$
	Random <sup>2</sup>	0.70	0.91	0.0154	0.00	0.06	0.0046	0.20	0.09	0.0129	0.50	0.54	0.0568
	MAP <sup>2</sup> V	90.05	73.14	0.9337	88.98	79.22	0.7723	92.50	83.05	0.7787	90.54	80.41	0.7636
	Ours	<b>90.30</b>	<b>74.51</b>	<b>0.9917</b>	<b>98.55</b>	<b>94.72</b>	<b>0.9834</b>	<b>98.55</b>	<b>92.87</b>	<b>0.9774</b>	<b>96.45</b>	<b>84.42</b>	<b>0.9794</b>

<sup>1</sup> Upper bound: similarity between ground-truth identity pairs (true target faces). <sup>2</sup> Lower bound: similarity from randomly generated faces without targeted reconstruction. <sup>3</sup> Average cosine similarity (on the target model) between target embeddings and final reconstructions. Values closer to the confidence threshold  $\tau_C$  indicate better convergence. **Bold** indicates the highest identity recovery performance.

TABLE VII: Performance comparison of DiffMI with training-dependent baselines and the naive APGD + DDPM strategy.

Attack	Generator	Training-Free	Dataset	Target Model	Evaluation									
					FaceNet		ArcFace		DCTDP		PartialFace		Avg.	
					Type I	Type II	Type I	Type II	Type I	Type II	Type I	Type II	Type I	Type II
DSCasConv [15]	DeconvNet	✗	LFW	ArcFace	<b>97.10</b>	<u>90.42</u>	100.00	99.03	<b>99.90</b>	<b>97.16</b>	<b>99.50</b>	<b>93.21</b>	<b>99.13</b>	<b>94.96</b>
Shahreza <i>et al.</i> [17]	StyleGAN	✗			61.00	49.33	98.10	77.79	84.10	59.41	74.00	52.24	79.30	59.69
MAP <sup>2</sup> V [14]	StyleGAN	✓			67.60	60.40	100.00	99.42	97.10	83.78	91.20	73.27	88.98	79.22
APGD (Random)*	DDPM	✓			69.10	61.33	100.00	99.56	92.30	75.40	84.50	66.51	86.48	75.70
APGD (Top 1/1000)*	DDPM	✓			78.00	71.70	100.00	<u>99.63</u>	96.00	83.91	90.70	76.59	91.18	82.96
DiffMI (Ours)	DDPM	✓			<b>96.00</b>	<b>91.03</b>	100.00	<b>99.64</b>	<b>99.60</b>	<b>95.88</b>	<b>98.60</b>	<b>92.33</b>	<b>98.55</b>	<b>94.72</b>

Gray cells indicate evaluation on target models. **Bold** and underline denote the highest and second-highest identity recovery performance, respectively.

\* Direct APGD attacks in the DDPM latent space without additional strategies. “Top 1/1000” selects the best of 1,000 samples; “Random” uses one unfiltered sample.

**Takeaway:** (i) The training-dependent DeconvNet-based method [15] achieves slightly higher recovery accuracy than our DiffMI but requires **6.4 million queries, 1.5 days** of training on **two A100 80GB GPUs**, and produces a target-specific generator that generalizes only to ArcFace. (ii) Both DiffMI and the training-heavy DeconvNet significantly outperform GAN-based methods and the naive APGD + DDPM approach. (iii) The naive APGD + DDPM strategy exhibits severe overfitting to the target model, achieving near-perfect performance on the target but a substantial drop on non-target evaluations.

icantly more computationally efficient and broadly applicable than training-dependent approaches, we include comparisons for completeness. As summarized in Tab. I, most training-dependent model inversion attacks rely on DeconvNets or GANs. We select two recent representatives: a DeconvNet-based method [15] and a GAN-based method [17].

As shown in Tab. VII, despite being training-free, DiffMI matches the recovery performance of the DeconvNet-based method [15] and significantly outperforms the GAN-based method [17]. The DeconvNet approach attains a slightly higher Type II accuracy (0.24% above DiffMI) but at substantial cost: training its target-specific generator requires **1.5 days** on **two A100 80GB GPUs** and **6.4 million queries** for gradient computation (ours costs 98–256 seconds and 1,300 queries per image for any model). Moreover, the generator is usable only for the target model it was trained on (ArcFace in Tab. VII); for any new target, the entire costly training process must be repeated. In contrast, DiffMI is fully training-free and applies directly to any face recognition model, requiring only 98–256 seconds and 1,300 queries per image.

Despite its computational burden, the DeconvNet method is limited to generating low-resolution (112 × 112) images. Furthermore, as illustrated in Fig. 9, it produces the lowest vi-

sual fidelity among all methods, yielding blurry and low-detail reconstructions. These limitations underscore the practical advantages of training-free methods, especially those leveraging expressive and resolution-flexible generative backbones such as GANs or diffusion models.

4) *Comparison with Naive APGD + DDPM:* A straightforward approach to applying diffusion models for training-free model inversion is to directly run adversarial attacks (*e.g.*, APGD [45]) in the latent space of an unconditional DDPM. However, this naive combination leads to severe artifacts and overfitting on the target model. These concerns are empirically validated in Tab. VII and Fig. 9.

As shown in Tab. VII, the naive “APGD + DDPM” strategy attains near-perfect Type II accuracy on the target model (approaching 100%) but suffers large drops on non-target models, ranging from −27.93% to −15.72%. In contrast, our controlled diffusion manipulation method limits this gap to −8.61% to −3.76%, demonstrating superior robustness and transferability. Notably, non-target model results are typically lower than those of the target model.

Moreover, as visualized in Fig. 9, applying APGD directly in the DDPM latent space introduces severe artifacts, even when initialized from the top-1 latent code among 1,000

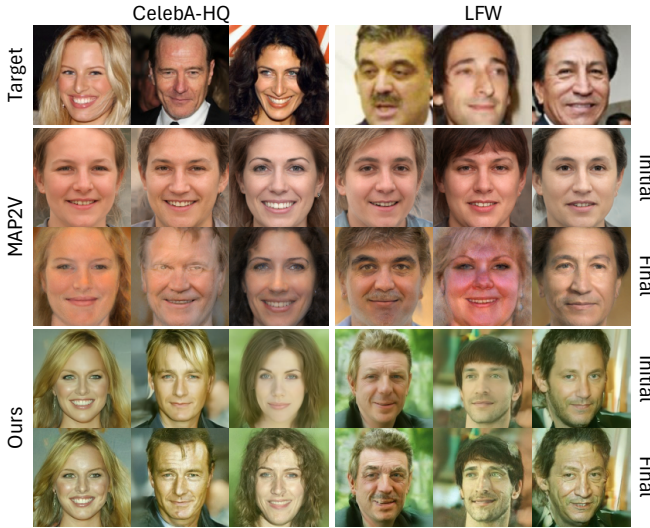


Fig. 8: Visual comparison of our DiffMI and MAP<sup>2</sup>V [14] in the white-box setting. DiffMI achieves higher identity recovery accuracy and produces full headshot-style reconstructions. “Initial” refers to outputs before manipulation. The target model is the inversion-resilient PartialFace [13].

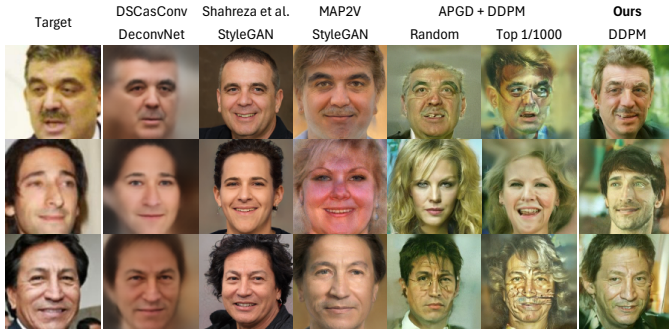


Fig. 9: Visual fidelity comparison across all baselines. Both Shahreza *et al.* [17] and our method produce high-resolution, headshot-style reconstructions with strong perceptual quality. In contrast, DSCasConv [15] yields low-resolution, blurry outputs with diminished facial detail. Naively applying APGD in the DDPM latent space results in severe artifacts, even when initialized from the top-1 latent code among 1,000 candidates.

candidates. These results further support the necessity of principled latent manipulation rather than naive adversarial optimization.

### B. Black-Box Model Inversion

We evaluate DiffMI in the black-box setting under various adversarial attack algorithms and compare its performance to the white-box variant. As shown in Fig. 10 (columns 3 vs. 10), GreedyPixel achieves Type II accuracy slightly lower than white-box APGD at higher query cost.

Fig. 10 (columns 4–6) further demonstrates that only fine-grained black-box methods such as GreedyPixel can effectively manipulate the diffusion model’s latent codes. In contrast, coarser strategies like Square [49] and BruSLe [50] fail to produce successful reconstructions.

TABLE VIII: Performance (%) with and without the confidence-aware objective.

Confidence-Aware	Time (s) ↓	Type II (%) ↑
✓ (ours)	<b>256</b>	84.42
✗	530	<b>85.31</b>

**Bold** indicates the best performance. The confidence-aware objective reduces runtime by over 50% with marginal accuracy loss.

TABLE IX: Ablation of the confidence threshold  $\tau_C$ .

Threshold $\tau_C$	Time (s) ↓	Similarity ↑	Type II (%) ↑
0.70	<b>23</b>	0.7294	69.93
0.80	38	0.8204	77.59
0.90	64	0.9111	83.11
0.97	213	0.9712	84.23
0.98 (from Eq. (8))	256	0.9794	84.42
0.99	442	<b>0.9861</b>	<b>84.98</b>

**Bold** indicates the best observed value per metric.

Finally, comparing columns 6–10, increasing the query budget and relaxing sparsity constraints improves inversion performance by allowing modification of more latent dimensions, yielding more accurate identity recovery.

## V. ABLATION STUDY

We conduct ablation studies on DiffMI using the LFW [39] dataset with inversion-resilient PartialFace [13] as the target model. Only Type II accuracy is reported, as it offers a more rigorous evaluation than Type I.

### A. Confidence-Aware Objective

We incorporate a confidence-aware objective into the ranked adversary strategy, enabling early stopping once a reconstruction exceeds a defined confidence threshold. This prioritizes highly-aligned latent codes and avoids unnecessary computation. As shown in Tab. VIII, the proposed objective significantly reduces runtime with only a minor decrease in Type II accuracy, offering an effective trade-off between efficiency and attack performance.

The confidence threshold  $\tau_C$ , defined in Eq. (8), specifies the similarity required for early termination. It serves as a soft upper bound, statistically estimated from real facial images. To ensure robustness,  $\tau_C$  should be significantly greater than the decision threshold  $\tau_F$ , but not excessively high (*e.g.*,  $\tau_C = 1$ ), which may increase computational cost.

As shown in Tab. IX, lower  $\tau_C$  values (*e.g.*,  $< 0.90$ ) yield faster attacks but reduce identity recovery, whereas higher values (*e.g.*,  $\tau_C > 0.98$ ) offer marginal accuracy gains at substantially higher runtime. Empirically,  $\tau_C = 0.98$  (from Eq. (8)) provides a strong balance between performance and efficiency. DiffMI is not highly sensitive to  $\tau_C$ ; even  $\tau_C = 0.90$  offers a reasonable trade-off. The threshold should avoid being set too low or too close to 1.0, with Eq. (8) serving as a statistical guideline rather than a strict requirement.

### B. Robustness of Latent Codes

As illustrated in Fig. 11, the normality of randomly sampled codes varies, with higher normality generally correlating with

1.Target	Pre-Manipulation		White-box Attack								Black-Box Attack							
	2.Top-1 Initial	3.APGD	4.Square	5.BruSLe	6.GreedyPixel	7.GreedyPixel	8.GreedyPixel	9.GreedyPixel	10.GreedyPixel	6.GreedyPixel	7.GreedyPixel	8.GreedyPixel	9.GreedyPixel	10.GreedyPixel				
Magnitude $\epsilon$	N/A	L2-norm $\epsilon = 35$	L2-norm $\epsilon = 35$	Unlimited	Unlimited	Unlimited	Unlimited	Unlimited	Unlimited	10%	10%	10%	10%	10%	10%	10%	10%	
Sparsity	Unlimited	Unlimited	Unlimited	30%	10%	10%	10%	10%	10%	50,000	50,000	100,000	200,000	200,000	200,000	200,000	200,000	
Max. Queries	1,000	1,100	20,000	20,000	20,000	50,000	100,000	200,000	200,000	200,000	200,000	200,000	200,000	200,000	200,000	200,000	200,000	
Type II (%) $\uparrow$	6.5	85.4	1.1	32.2	41.1	67.8	76.7	80.0	81.1									

Fig. 10: Performance of DiffMI in the black-box setting. Compared to its white-box counterpart (columns 3 vs. 10), black-box DiffMI achieves slightly lower Type II accuracy. Among black-box methods (columns 4–6), only the fine-grained GreedyPixel algorithm successfully manipulates the diffusion model’s latent codes. Columns 6–10 show that increasing the attack budget (queries and sparsity) improves inversion performance. Notably, 40% of identities become recognizable after just 20,000 queries, with diminishing returns beyond 100,000. The dataset is LFW, the target model is the inversion-resilient PartialFace [13], and evaluation is performed using ArcFace [11].

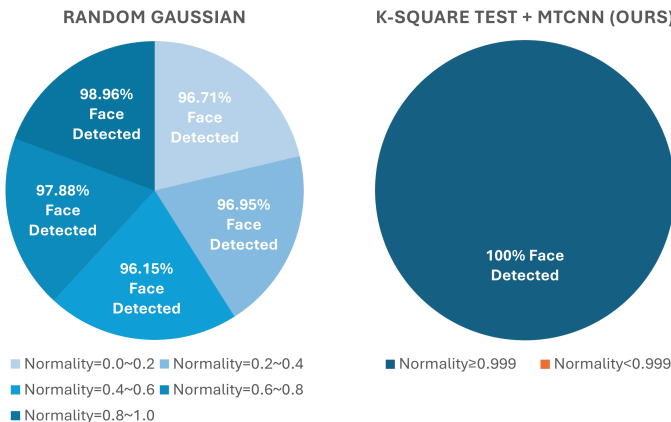


Fig. 11: Quality of randomly generated latent codes and effectiveness of the proposed selection strategy. In the left subfigure, Gaussian normality varies across samples, with higher normality generally correlating with improved face detection rates (darker regions). In the right subfigure, our two-stage strategy enforces  $100\% p_K \geq 0.999$  and consistently achieves a 100% face detection rate ( $p_D \geq 0.999$ ).

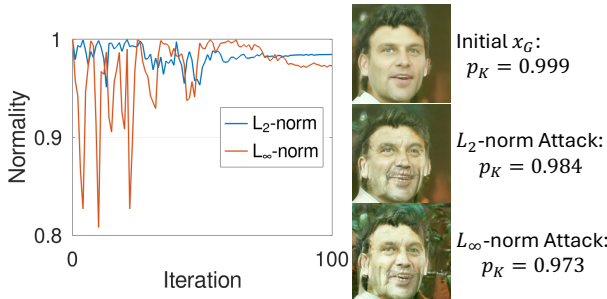


Fig. 12: Impact of adversarial manipulation on Gaussian normality.  $L_2$ -constrained adversaries better preserve latent normality than  $L_\infty$ -constrained ones, resulting in improved reconstruction fidelity.

higher face detection rates. However, as shown in Fig. 12, even highly normal codes can lose normality after adversarial



Fig. 13: Examples of failed face generation from randomly sampled latent codes. MTCNN fails to detect a face, resulting in detection confidence  $p_D = 0$ .

TABLE X: Ablation of latent code selection strategies.

Strategy	Time (s) $\downarrow$	Type II (%) $\uparrow$
Random Gaussian	290	82.78
$K^2$ Test	293	82.47
$K^2$ Test + MTCNN (ours)	<b>256</b>	<b>84.42</b>

**Bold** indicates the superiority of our strategy.

manipulation, with greater distortion leading to more severe visual artifacts. Moreover, as shown in Fig. 13, latent codes satisfying Gaussian normality may still fail to produce recognizable faces. These distortion and failure cases underscore the importance of our strategy in guaranteeing optimal initialization, ensuring that 100% of samples meet  $p_K \geq 0.999$  and all facial regions are detected. As shown in Tab. X, our strategy, combining  $K^2$  test with MTCNN face detection, produces the most robust latent codes, improving Type II accuracy and reducing runtime.

### C. Top- $N$ Selection

As demonstrated in Fig. 14, selecting the code with highest initial similarity can underperform after adversarial optimization. Therefore, DiffMI selects the top  $N$  latent codes, improving efficiency through a ranked adversary strategy without processing all candidates. As shown in Tab. XI, larger  $N$  increases Type II accuracy at the cost of longer runtime.

Target	Initial	Final		
			Similarity $\uparrow$	0.2887 0.2831 0.9284 0.9817
Rank	Top-1	Top-2	Top-2	Top-1

Fig. 14: Example where the latent code with the best initial reconstruction fails to achieve the highest final similarity after adversarial optimization.

TABLE XI: Ablation of the top- $N$  value in latent code selection.

Top $N$	Time (s) $\downarrow$	Type II (%) $\uparrow$
1	<b>189</b>	81.06
3	256	84.42
5	289	<b>85.21</b>

**Bold** indicates the best performance. Increasing  $N$  improves reconstruction quality but incurs higher computational cost.

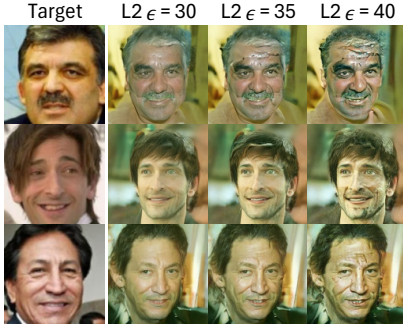


Fig. 15: Larger perturbations introduce stronger artifacts, increasing visible noise and reducing generation realism.

TABLE XII: Ablation of perturbation constraints across different norms and magnitudes.

Norm	Magnitude $\epsilon$	Time (s) $\downarrow$	Similarity $\uparrow$	Type II (%) $\uparrow$
$L_2$	30	455	0.9707	81.49
$L_2$	35	256	0.9794	84.42
$L_2$	40	<b>191</b>	<b>0.9816</b>	<b>86.11</b>
$L_\infty$	0.15	260	0.9791	75.28

**Bold** indicates the best result per metric.

#### D. Perturbation Constraint

As shown in Fig. 12,  $L_2$ -norm-constrained adversaries better preserve distributional normality compared to their  $L_\infty$  counterparts, resulting in higher-fidelity reconstructions. This is supported by Tab. XII, where  $L_2$  and  $L_\infty$  attacks yield similar similarity scores, but the  $L_2$  constraint ( $\epsilon = 35$ ) achieves substantially higher accuracy.

While Tab. XII suggests that increasing  $\epsilon$  leads to improved accuracy and reduced runtime, Fig. 15 reveals a trade-off: larger perturbation magnitudes introduce stronger visual artifacts, degrading perceptual quality. Thus, the optimal  $\epsilon$  must balance reconstruction effectiveness with visual naturalness.

## VI. CONCLUSION

We present DiffMI, the first diffusion-driven, training-free model inversion attack against embedding-based face recognition systems. Unlike prior methods relying on GANs or target-specific training, DiffMI manipulates latent codes of an unconditional diffusion model to produce high-fidelity, identity-preserving reconstructions.

Extensive white-box and black-box evaluations show that DiffMI compromises diverse face recognition models, including those designed for inversion resistance. It consistently outperforms existing training-free baselines and approaches the performance of training-dependent attacks, without target-specific training or generator tuning. A user study further validates the perceptual realism of our reconstructions.

DiffMI incorporates key algorithmic components: confidence-aware early stopping, statistical latent code selection, and Ranked Adversary optimization, which balance query efficiency and reconstruction quality. Ablation studies confirm the contribution of each design choice.

Our findings suggest that model inversion is inherently difficult to defend due to its reliance on inference-time behavior. If a face recognition system excels at identity matching, it may be intrinsically vulnerable to inversion. Future work should explore stronger defenses against training-free attacks, particularly those leveraging high-fidelity generative priors. The safe deployment of such models in privacy-sensitive applications also warrants deeper study, including robust inversion detection, mitigation strategies, and privacy-preserving architectures.

## REFERENCES

- [1] Office of Inspector General, Department of Homeland Security, “Review of cbp’s major cybersecurity incident during a 2019 biometric pilot,” Tech. Rep. OIG-20-71, U.S. Department of Homeland Security, Office of Inspector General, Sept. 2020. Accessed: 2025-08-12.
- [2] J. Taylor, “Major breach found in biometrics system used by banks, uk police and defence firms,” Aug. 2019. The Guardian. Accessed: 2025-08-12.
- [3] Fortune Staff, “The shanghai data leak shows china’s state surveillance was inevitable,” July 2022. Fortune. Accessed: 2025-08-12.
- [4] C. Burt, “Reported australian biometric data breach prompts arrest and hysteria,” May 2024. Biometric Update. Accessed: 2025-08-12.
- [5] P. A. Thomas, “Data leak exposes personal data of indian military and police,” May 2024. CSO Online. Accessed: 2025-08-12.
- [6] Microsoft, *Face API Reference*, 2024. Azure AI Services Documentation.
- [7] A. W. Services, *Amazon Rekognition Documentation*, 2024. AWS Documentation.
- [8] G. Cloud, *Cloud Vision Documentation*, 2024. Google Cloud Documentation.
- [9] Face++, *Face++ Documentation*, 2024. Face++ Official Documentation.
- [10] F. Schroff, D. Kalenichenko, and J. Philbin, “Facenet: A unified embedding for face recognition and clustering,” in *Proceedings of the IEEE Conference on Computer Vision and Pattern Recognition (CVPR)*, (Boston, Massachusetts, USA), pp. 815–823, IEEE, 2015.
- [11] J. Deng, J. Guo, N. Xue, and S. Zafeiriou, “Arcface: Additive angular margin loss for deep face recognition,” in *Proceedings of the IEEE/CVF Conference on Computer Vision and Pattern Recognition (CVPR)*, (Long Beach, CA, USA), pp. 4690–4699, IEEE, 2019.
- [12] J. Ji, H. Wang, Y. Huang, J. Wu, X. Xu, S. Ding, S. Zhang, L. Cao, and R. Ji, “Privacy-preserving face recognition with learnable privacy budgets in frequency domain,” in *European Conference on Computer Vision (ECCV)*, (Tel Aviv, Israel), pp. 475–491, Springer, 2022.

- [13] Y. Mi, Y. Huang, J. Ji, M. Zhao, J. Wu, X. Xu, S. Ding, and S. Zhou, "Privacy-preserving face recognition using random frequency components," in *Proceedings of the IEEE/CVF International Conference on Computer Vision (ICCV)*, pp. 19673–19684, IEEE, 2023.
- [14] H. Zhang, X. Dong, Y. Lai, Y. Zhou, X. Zhang, X. Lv, Z. Jin, and X. Li, "Validating privacy-preserving face recognition under a minimum assumption," in *Proceedings of the IEEE/CVF Conference on Computer Vision and Pattern Recognition (CVPR)*, (Seattle, Washington, United States), pp. 12205–12214, IEEE, 2024.
- [15] H. O. Shahreza, V. K. Hahn, and S. Marcel, "Vulnerability of state-of-the-art face recognition models to template inversion attack," *IEEE Transactions on Information Forensics and Security*, 2024.
- [16] H. O. Shahreza and S. Marcel, "Face reconstruction from facial templates by learning latent space of a generator network," *Advances in Neural Information Processing Systems (NIPS)*, vol. 36, 2023.
- [17] H. O. Shahreza and S. Marcel, "Template inversion attack using synthetic face images against real face recognition systems," *IEEE Transactions on Biometrics, Behavior, and Identity Science*, 2024.
- [18] X. Dong, Z. Miao, L. Ma, J. Shen, Z. Jin, Z. Guo, and A. B. J. Teoh, "Reconstruct face from features based on genetic algorithm using gan generator as a distribution constraint," *Computers & Security*, vol. 125, p. 103026, 2023.
- [19] M. Fredrikson, S. Jha, and T. Ristenpart, "Model inversion attacks that exploit confidence information and basic countermeasures," in *Proceedings of the 22nd ACM SIGSAC Conference on Computer and Communications Security (ACM CCS)*, pp. 1322–1333, 2015.
- [20] G. Mai, K. Cao, P. C. Yuen, and A. K. Jain, "On the reconstruction of face images from deep face templates," *IEEE Transactions on Pattern Analysis and Machine Intelligence*, vol. 41, no. 5, pp. 1188–1202, 2018.
- [21] Z. Zhang, X. Wang, J. Huang, and S. Zhang, "Analysis and utilization of hidden information in model inversion attacks," *IEEE Transactions on Information Forensics and Security*, 2023.
- [22] C. N. Duong, T.-D. Truong, K. Luu, K. G. Quach, H. Bui, and K. Roy, "Vec2face: Unveil human faces from their blackbox features in face recognition," in *Proceedings of the IEEE/CVF Conference on Computer Vision and Pattern Recognition*, pp. 6132–6141, 2020.
- [23] Y. Zhang, R. Jia, H. Pei, W. Wang, B. Li, and D. Song, "The secret revealer: Generative model-inversion attacks against deep neural networks," in *Proceedings of the IEEE/CVF Conference on Computer Vision and Pattern Recognition (CVPR)*, pp. 253–261, 2020.
- [24] M. Khosravy, K. Nakamura, Y. Hirose, N. Nitta, and N. Babaguchi, "Model inversion attack by integration of deep generative models: Privacy-sensitive face generation from a face recognition system," *IEEE Transactions on Information Forensics and Security*, vol. 17, pp. 357–372, 2022.
- [25] X. Yuan, K. Chen, J. Zhang, W. Zhang, N. Yu, and Y. Zhang, "Pseudo label-guided model inversion attack via conditional generative adversarial network," in *Proceedings of the AAAI Conference on Artificial Intelligence (AAAI)*, vol. 37, pp. 3349–3357, 2023.
- [26] B.-N. Nguyen, K. Chandrasegaran, M. Abdollahzadeh, and N.-M. M. Cheung, "Label-only model inversion attacks via knowledge transfer," *Advances in Neural Information Processing Systems (NIPS)*, vol. 36, 2023.
- [27] J. Wu, C. Wan, H. Chen, Z. Zheng, and Y. Sun, "Label-only model inversion attacks: Adaptive boundary exclusion for limited queries," *Neurocomputing*, p. 129902, 2025.
- [28] M. Kansy, A. Raël, G. Mignone, J. Naruniec, C. Schroers, M. Gross, and R. M. Weber, "Controllable inversion of black-box face recognition models via diffusion," in *Proceedings of the IEEE/CVF International Conference on Computer Vision (ICCV) Workshops*, pp. 3167–3177, 2023.
- [29] R. Liu, D. Wang, Y. Ren, Z. Wang, K. Guo, Q. Qin, and X. Liu, "Unstoppable attack: Label-only model inversion via conditional diffusion model," *IEEE Transactions on Information Forensics and Security*, 2024.
- [30] L. Struppek, D. Hintersdorf, A. D. A. Correira, A. Adler, and K. Kersting, "Plug & play attacks: Towards robust and flexible model inversion attacks," in *International Conference on Machine Learning (ICML)*, pp. 20522–20545, PMLR, 2022.
- [31] Y. Qiu, H. Fang, H. Yu, B. Chen, M. Qiu, and S.-T. Xia, "A closer look at gan priors: Exploiting intermediate features for enhanced model inversion attacks," in *European Conference on Computer Vision (ECCV)*, pp. 109–126, Springer, 2024.
- [32] S. Pang, Y. Rao, Z. Lu, H. Wang, Y. Zhou, and M. Xue, "Pridm: Effective and universal private data recovery via diffusion models," *IEEE Transactions on Dependable and Secure Computing*, 2025.
- [33] Z. Boulkenafet, J. Komulainen, L. Li, X. Feng, and A. Hadid, "Oulu-npu: A mobile face presentation attack database with real-world variations," in *2017 12th IEEE international conference on automatic face & gesture recognition (FG 2017)*, pp. 612–618, IEEE, 2017.
- [34] M. Tan, Z. Zhou, and Z. Li, "The many-faced god: Attacking face verification system with embedding and image recovery," in *Proceedings of the 37th Annual Computer Security Applications Conference (ACSAC)*, pp. 17–30, 2021.
- [35] R. Rombach, A. Blattmann, D. Lorenz, P. Esser, and B. Ommer, "High-resolution image synthesis with latent diffusion models," in *Proceedings of the IEEE/CVF Conference on Computer Vision and Pattern Recognition (CVPR)*, pp. 10684–10695, 2022.
- [36] T. Karras, S. Laine, M. Aittala, J. Hellsten, J. Lehtinen, and T. Aila, "Analyzing and improving the image quality of stylegan," in *Proceedings of the IEEE/CVF Conference on Computer Vision and Pattern Recognition (CVPR)*, pp. 8110–8119, 2020.
- [37] C. Meng, Y. He, Y. Song, J. Song, J. Wu, J.-Y. Zhu, and S. Ermon, "SDEdit: Guided image synthesis and editing with stochastic differential equations," in *International Conference on Learning Representations (ICLR)*, 2022.
- [38] C.-H. Lee, Z. Liu, L. Wu, and P. Luo, "Maskgan: Towards diverse and interactive facial image manipulation," in *IEEE Conference on Computer Vision and Pattern Recognition (CVPR)*, 2020.
- [39] G. B. Huang, M. Mattar, T. Berg, and E. Learned-Miller, "Labeled faces in the wild: A database for studying face recognition in unconstrained environments," in *Workshop on Faces in 'Real-Life' Images: Detection, Alignment, and Recognition*, 2008.
- [40] R. B. D'Agostino, "Transformation to normality of the null distribution of  $g_1$ ," *Biometrika*, vol. 57, no. 3, pp. 679–681, 1970.
- [41] R. D'agostino and E. S. Pearson, "Tests for departure from normality. empirical results for the distributions of  $b^2$  and  $\sqrt{b^1}$ ," *Biometrika*, vol. 60, no. 3, pp. 613–622, 1973.
- [42] R. B. D'agostino, A. Belanger, and R. B. D'Agostino Jr, "A suggestion for using powerful and informative tests of normality," *The American Statistician*, vol. 44, no. 4, pp. 316–321, 1990.
- [43] K. Zhang, Z. Zhang, Z. Li, and Y. Qiao, "Joint face detection and alignment using multitask cascaded convolutional networks," *IEEE Signal Processing Letters*, vol. 23, no. 10, pp. 1499–1503, 2016.
- [44] H. Wang, C.-C. Chang, C.-S. Lu, C. Leckie, and I. Echizen, "Greedy-pixel: Fine-grained black-box adversarial attack via greedy algorithm," *arXiv preprint arXiv:2501.14230*, 2025.
- [45] F. Croce and M. Hein, "Reliable evaluation of adversarial robustness with an ensemble of diverse parameter-free attacks," in *International Conference on Machine Learning (ICML)*, pp. 2206–2216, 2020.
- [46] Q. Cao, L. Shen, W. Xie, O. M. Parkhi, and A. Zisserman, "Vggface2: A dataset for recognising faces across pose and age," in *2018 13th IEEE International Conference on Automatic Face & Gesture Recognition (FG 2018)*, pp. 67–74, IEEE, 2018.
- [47] Y. Guo, L. Zhang, Y. Hu, X. He, and J. Gao, "Ms-celeb-1m: A dataset and benchmark for large-scale face recognition," in *14th European Conference on Computer Vision (ECCV)*, pp. 87–102, Springer, 2016.
- [48] T. Karras, S. Laine, and T. Aila, "A style-based generator architecture for generative adversarial networks," in *Proceedings of the IEEE/CVF Conference on Computer Vision and Pattern Recognition (CVPR)*, pp. 4401–4410, 2019.
- [49] M. Andriushchenko, F. Croce, N. Flammarion, and M. Hein, "Square attack: a query-efficient black-box adversarial attack via random search," in *European Conference on Computer Vision (ECCV)*, pp. 484–501, 2020.
- [50] Q. V. Vo, E. Abbasnejad, and D. Ranasinghe, "Brusleattack: Query-efficient score-based sparse adversarial attack," in *The Twelfth International Conference on Learning Representations (ICLR)*, 2024.
- [51] Malwarebytes Labs, "Billions of logins for apple, google, facebook, telegram, and more found exposed online," June 2025. Accessed: 2025-08-06.
- [52] H. Wang, S. Wang, Z. Jin, Y. Wang, C. Chen, and M. Tistarelli, "Similarity-based gray-box adversarial attack against deep face recognition," in *2021 16th IEEE International Conference on Automatic Face and Gesture Recognition (FG 2021)*, pp. 1–8, IEEE, 2021.
- [53] H. Wang, S. Wang, C. Chen, M. Tistarelli, and Z. Jin, "A multi-task adversarial attack against face authentication," *ACM Transactions on Multimedia Computing, Communications and Applications*, vol. 20, no. 11, pp. 1–24, 2024.

In this supplementary document, we provide additional materials to further support the design rationale and enhance the readability of the main manuscript.

*a) Comprehensive Discussions on Key Topics:* We offer in-depth discussions that complement and extend the main text:

- Why Model Inversion is Dangerous and Realistic in Face Recognition?
- Why Embedding-Based Open-Set Recognition over Closed-Set Classification?
- Why Prefer Diffusion Over GAN-based Inversion?
- Why Not Naive APGD + DDPM?
- Why We Target Identity Consistency Instead of Pixel-Level Reconstruction?
- Why Compare with These Baselines?
- Why Our Quantitative Evaluation is Fair?
- Why Model Inversion is Hard to Defend?

*b) Diversity of Model Architectures and Datasets:* We demonstrate the robustness and generality of our findings across diverse architectures and datasets.

*c) Notations and Corresponding Definitions:* We summarize all mathematical symbols and their definitions for clarity and consistency.

## APPENDIX A DISCUSSION

### A. Why Model Inversion is Dangerous and Realistic in Face Recognition?

Modern face recognition systems, used in authentication, surveillance, and identity verification, increasingly adopt an embedding-based paradigm. Instead of storing raw images, they encode inputs into compact embeddings and compare them via cosine or Euclidean similarity, improving scalability, supporting open-set recognition, and enabling efficient retrieval [6]–[9].

*a) Embeddings are assumed to be privacy-preserving:* Because embeddings abstract pixel-level details, they are often viewed as anonymized or non-invertible. Many systems treat them as safe to store, transmit, or expose to clients. However, embeddings retain semantically rich identity features and can be inverted under adversarial conditions.

*b) Model inversion reveals reconstruction feasibility:* Recent studies show that expressive deep models allow embeddings to be used for reconstructing visually realistic, identity-preserving faces [14]. Such attacks can synthesize high-fidelity headshot-style images from embeddings alone, without identity labels or training data.

*c) Biometric data are non-revocable:* Unlike passwords or cryptographic keys, embeddings encode immutable biometric traits. Once compromised (via client-side memory leaks, inference API exposure, or intermediate model output) they cannot be revoked or re-issued. Even partial leakage enables spoofing, synthetic ID forgery, or impersonation [33], [34].

*d) Embedding leakage is a practical concern:* Many commercial services expose embeddings or similarity scores via SDKs or web APIs. Black-box leakage arises when similarity scores are returned to clients; white-box leakage occurs

through insecure deployment, shared inference servers, or side-channel access. Embeddings are often stored in databases for caching, retrieval, or verification, yet these may be compromised via breaches or insider threats (e.g., third-party SDKs, optional cloud APIs, misconfigured backups) [1]–[5], [51]. Frequently stored unencrypted and deemed “non-sensitive,” such leaks often go unnoticed, enabling inversion without access to training data or labels.

**Summary** Model inversion attacks against embedding-based face recognition are technically feasible and practically relevant. Because embeddings are semantically rich, hard to protect, and irreversible once leaked, they represent a critical security and privacy risk. Mitigating this requires moving beyond the assumption of “embedding-level privacy.”

### B. Why Embedding-Based Open-Set Recognition over Closed-Set Classification?

Modern face recognition systems are fundamentally embedding-based in both research and deployment, driven by advantages over traditional classification-based approaches.

*a) Scalability and generalization to unseen identities:* Embedding-based models enable open-set recognition. Instead of training on a fixed set of classes, models such as FaceNet [10] and ArcFace [11] map facial images into a continuous embedding space, where similarity is computed using metrics like cosine or Euclidean distance. This allows new identities to be enrolled dynamically without retraining.

*b) Industry-wide adoption:* Commercial platforms including Microsoft Azure [6], Amazon Rekognition [7], and Google Cloud Vision [8] widely employ embedding-based pipelines. In these systems, embeddings serve as the core representation for matching, verification, and search, often as the final stored artifact tied to user identity.

**Summary** Given their central role, embeddings are the primary target in model inversion attacks. Focusing on embeddings aligns with both dominant industry practice and realistic threat models, where raw images are discarded but embeddings are retained for long-term identity recognition.

### C. Why Prefer Diffusion Over GAN-based Inversion?

*a) No truncation bottleneck:* GAN-based inversion, particularly with StyleGAN [36], typically operates in the intermediate latent space  $\mathcal{W}$ , obtained by mapping standard Gaussian noise from the original latent space  $\mathcal{Z}$  through a learned multilayer perceptron (MLP). The disentangled  $\mathcal{W}$  space allows more controllable and realistic synthesis. To suppress unnatural outputs, the truncation trick restricts latent codes to a narrow radius around the mean in  $\mathcal{W}$ . While improving visual quality, truncation reduces expressiveness by excluding low-density regions of the latent space (crucial for reconstructing diverse or atypical identities). In contrast, DDPMs generate images by progressively denoising Gaussian noise without adhering to a fixed latent distribution, enabling unconstrained yet coherent exploration of the generative space and avoiding the realism–diversity trade-off imposed by truncation.

*b) Higher-dimensional, disentangled latent space:*

DDPMs operate in a high-dimensional, near-isotropic latent space ( $\sim 200K$  dimensions for  $3 \times 256 \times 256$  images), offering far greater flexibility than StyleGAN's  $\sim 512$ -dimensional  $\mathcal{W}$  space. This facilitates fine-grained controls and mitigates the entanglement common in lower-dimensional representations.

*c) Controlled optimization:*

Our pipeline integrates on-manifold initialization (robust latent codes), identity-aware warm starts (top  $N$  selection), and confidence-aware optimization (ranked adversary with early stopping). These strategies constrain updates to remain within high-probability regions of the diffusion prior, thereby preserving image realism throughout the optimization process.

**Summary** A well-controlled DDPM enables precise, artifact-resistant manipulation while maintaining generative realism, surpassing GAN-based methods constrained by truncation and latent entanglement (see evidence in Tab. VI).

#### D. Why Not Naive APGD + DDPM?

*a) Manifold mismatch:*

Diffusion models are trained to map Gaussian noise to the natural image manifold. However, APGD [45] introduces perturbations that drive latent vectors off this manifold. These deviations are *amplified* during the denoising process, leading to visual artifacts such as halos, patchy textures, and double contours.

*b) Identity-agnostic initialization:*

Because the initial noise is sampled independently of the target identity, APGD requires a large perturbation budget to steer the generation toward the desired embedding. This extended traversal increases the likelihood of optimization artifacts.

*c) Lack of transferability:*

Naive APGD aggressively overfits to the target model by fully maximizing embedding similarity, even at the cost of introducing more artifacts. As a result, the generated images often fail to generalize to non-target recognition models, reducing cross-model robustness.

**Summary** The unconstrained optimization of the naive "APGD + DDPM" undermines the diffusion prior that ensures generative realism (see evidence in Tab. VII and Fig. 9).

#### E. Why We Target Identity Consistency Instead of Pixel-Level Reconstruction?

A key question in model inversion attacks is whether the objective should be reconstructing the *identical* input image or merely recovering the *identity* of the target. We argue that targeting **identity-consistent** outputs is both theoretically justified and practically sufficient for evaluating privacy risks.

*a) Privacy leakage centers on identity:*

Face recognition systems use embeddings to match identities, not pixel-level details. Thus, reconstructing any image perceived as the same person, even with variations in pose, lighting, or background, constitutes a privacy breach. This reflects realistic threats such as re-identification, impersonation, or spoofing using generated media. The privacy risk arises not from exact replication of an image, but from revealing the individual's identity.

*b) Theoretical limitations of exact recovery:*

Recovering the *exact* input image from its embedding is fundamentally ill-posed. Models such as ArcFace and FaceNet compress high-dimensional facial images into low-dimensional embeddings (e.g., 512D), discarding information irrelevant to identity. This many-to-one mapping means multiple images of the same person collapse to nearly identical embeddings. Exact pixel-wise inversion is therefore unnecessary and, in many cases, *impossible* due to this dimensionality bottleneck.

*c) Practical threat scenario:*

This perspective aligns with realistic threat models. In applications such as surveillance, authentication, or forensic recovery, attackers seek to learn or impersonate a person's identity, not retrieve a specific photo. Privacy-preserving mechanisms should thus be evaluated by their ability to prevent identity inference from embeddings rather than exact image recovery.

**Summary** DiffMI adopts identity-preserving reconstruction as its primary objective, consistent with the theory of embedding-based systems and the real-world threats model inversion aims to assess. Our method targets the privacy leakage most relevant to face recognition systems: *who* the person is, not *how* they look in a specific image.

#### F. Why Compare with These Baselines?

*a) Two categories of existing methods:*

As summarized in Tab. I, existing model inversion attacks against face recognition can be grouped into *training-dependent* methods (based on DeconvNet, GANs, or diffusion models) and *training-free* methods (primarily GAN-based, or our proposed diffusion-driven approach).

*b) Primary baseline:*

Our main comparison is with MAP<sup>2</sup>V [14], a recent, highly relevant training-free GAN-based attack.

*c) Representative training-dependent methods:*

For completeness, we also evaluate representative training-dependent methods based on DeconvNet and GANs [15], [17]. While not primary baselines due to their substantial training overhead, they serve as benchmarks to highlight the efficiency of training-free approaches.

*d) Naive diffusion-based baseline:*

To contextualize our pipeline's benefits, we evaluate a naive baseline that applies APGD directly to DDPM without our initialization, ranking, or confidence-aware mechanisms. This mimics a straightforward adaptation of GAN-based attacks to the diffusion domain, optimizing latent codes purely via gradient ascent on similarity.

*e) Excluded tasks:*

We exclude closed-set classification attacks, which require task-specific training on a fixed set of identities and apply only to seen identities and models, contrary to our focus on unseen cases.

*f) Excluded partial-image attacks:*

We also exclude PriDM [32], which requires partial target images and thus demands more information than allowed under our threat model.

**Summary** Our benchmark selection balances training-free and training-dependent paradigms while adhering strictly to our threat model.

### G. Why Our Quantitative Evaluation is Fair?

a) *Avoiding adversarial overfitting:* A key challenge in evaluating model inversion attacks is avoiding inflated results from overfitting to the target model. Adversarial artifacts may exploit model-specific weaknesses, yielding high similarity scores without preserving meaningful identity features and thus misleading quantitative evaluations [52], [53].

b) *Non-target model evaluation:* To mitigate this, we follow a widely used protocol that measures identity similarity on *non-target* face recognition models not involved in optimization [14]–[18]. This ensures reconstruction success reflects transferable identity features rather than target-specific overfitting. A match across non-target models provides stronger evidence that the underlying identity is faithfully recovered.

c) *Alignment with real-world threats:* This protocol also matches realistic threat scenarios, where attackers aim to reconstruct biometric images capable of impersonating the same identity across different systems. Since biometric traits are immutable, a successful match on non-target models demonstrates a true privacy breach.

**Summary** Using non-target models yields a fair and privacy-relevant measure of reconstruction success.

### H. Why Model Inversion is Hard to Defend?

a) *Inference-time leakage is unavoidable:* Model inversion is inherently an inference-time threat. In embedding-based face recognition, attackers need only access to the model’s inputs and outputs (e.g., a query image and its embedding) to attempt reconstruction. This reflects common real-world deployments, such as mobile verification or cloud APIs, where embeddings are exposed for identification. As long as a system performs identity matching, an attacker can search for a reconstruction that matches the exposed embedding.

b) *Any high-matching reconstruction is a privacy breach:* For a given embedding, many images can yield high similarity. If reconstruction introduces uncontrolled artifacts, results may be unrecognizable or adversarial; but steering optimization to avoid artifacts often produces an image resembling the true identity. Thus, the ability of face recognition to generalize across pose and illumination inherently enables inversion.

c) *Embedding matching as a proxy for identity:* Embedding similarity correlates strongly with human-perceived identity. Systems are trained to produce similar embeddings for images of the same person despite variation. Therefore, finding an image that closely matches a target embedding recovers key facial characteristics of that person. If a system excels at recognition, it must also be invertible, an inherent tension.

d) *Gradient masking and training-time defenses are insufficient:* Techniques such as gradient hiding or privacy-aware training [12], [13] may reduce overfitting to training data but do not address the core issue: embeddings remain semantically meaningful and exposed at inference. Even without gradient access, query-based optimization can recover facial structure.

e) *Face recognition accuracy implies invertibility:* Paradoxically, the better a system is at identity recognition, the more vulnerable it is to inversion. If a model can reliably distinguish individuals, inverting its output can produce an image that must resemble the underlying person. This stems from the design of embedding spaces to preserve identity semantics.

**Summary** Model inversion is difficult to defend because it exploits core design principles of face recognition. As long as embeddings are exposed for matching and preserve identity in feature space, attackers can reconstruct the underlying identity. Mitigation requires rethinking how embeddings are generated and shared, rather than assuming safety from the absence of raw images.

## APPENDIX B NOTATIONS

The key notations and their corresponding definitions are summarized in Tab. XIII.

## APPENDIX C MODEL ARCHITECTURES AND DATASETS

We identify that training-dependent model inversion attacks incur high computational cost and limited generalizability due to their reliance on target-specific generator training. To address these limitations, we propose DiffMI, which leverages a fixed, unconditional diffusion model (DDPM) to attack unseen target identities and face recognition models without retraining.

For a comprehensive evaluation, we consider diverse model architectures and datasets, as summarized in Tab. II. The DDPM generator and the four recognition models differ substantially in both architecture and training data. Our primary evaluation uses LFW, which is excluded from training for both the generator and recognition models, ensuring all cross-model evaluations involve architectural and distributional mismatches.

We further investigate whether alignment between the generator’s training data and the attack domain improves reconstruction. This simulates a practical case where the attacker’s data distribution resembles the target’s (e.g., ID photos often share similar format and content). To this end, we select 1,000 target identities from CelebA-HQ (the dataset used to train DDPM) and compare results with LFW targets. As shown in Tab. IV, prior alignment yields only marginal improvements or even slight degradation in some cases (e.g., +2.82% accuracy on LFW vs. CelebA-HQ for DCTDP). These results suggest that, in training-free open-set inversion, alignment with the generator’s training distribution offers limited practical benefit.

Lastly, we examine whether our evaluation dataset size (1,000 images per dataset) is sufficient for a training-free method. Results in Tab. XIV show that performance stabilizes once the dataset size reaches 500 samples, as the change from 500 to 1,000 is only marginal. Therefore, as DiffMI is training-free, evaluation variance is largely independent of dataset size.

TABLE XIII: Key notations and their corresponding definitions.

Notation	Definition	Remark	Reference
$F(\cdot)$	Embedding function (Face recognition)	White- or black-box knowledge	
$x$	Facial image		
$z$	Feature Embedding		
$S(\cdot, \cdot)$	Similarity function (cosine)		
$T_F$	Similarity decision threshold		
$x^{tgt}$	Target facial image	Unknown to Attackers	
$z^{tgt}$	Target embedding, transformed from the target face	Known to Attackers	
$\hat{x}$	Reconstructed image	Attack Output	
$\hat{z}$	Feature embedding of the reconstructed image		Sec. II-C
$G(\cdot)$	Generative function (DDPM)	Pretrained, unconditional	
$x_G$	Latent code, drawn from a random Gaussian distribution	Attack Input	
$x'_G$	Manipulated latent code		
$\delta$	Adversarial perturbations on the latent code		
$\ \cdot\ _p$	$L_p$ -norm		
$\epsilon$	Perturbation magnitude	Attack Setting	
$\mathcal{L}$	Objective function		
$\tau_C$	Confidence threshold (sufficient similarity)	Attack Setting	
$K(\cdot)$	Gaussian normality test function ( $K^2$ test)		
$p_K$	Gaussian normality (the probability of following a normal distribution)		Sec. II-D1
$\tau_K$	Threshold of Gaussian normality	Attack Setting	
$D(\cdot)$	Face detection function (MTCNN)		
$p_D$	Face detection confidence score		Sec. II-D2
$\tau_D$	Threshold of detection confidence	Attack Setting	
$V$	Volume of reliable latent codes (Step (a))	Attack Setting	
$N$	Top $N$ selection (Step (b))	Attack Setting	Sec. II-E
$Q$	Query Efficiency		
$t_{max}$	Maximum iterations per adversarial attack	Attack Setting	
$Q_{max}$	Maximum number of queries (only for black-box attacks)	Attack Setting	Sec. II-F
$\lfloor \cdot \rfloor$	Floor function		
$\mathbb{I}(\cdot)$	Indicator function		
$I$	Total number of attack samples		
$x^{j \neq tgt}$	Facial images distinct from the target, associated with the same identity		Sec. III
$J$	Total number of $x^{j \neq tgt}$ for each identity		

TABLE XIV: Impact of dataset size on evaluation variance.

Size	Type I (%)	Gap	Type II (%)	Gap
100	98.00	1.00	91.59	2.77
200	99.00	0.45	94.36	0.22
500	98.55	0.00	94.58	0.14
1,000	98.55		94.72	

Target model: ArcFace [11]; evaluation dataset: LFW [39].